ORIGINAL PAPER

Optimal Homotopy Asymptotic Solution for Cross-Diffusion Effects on Slip Flow and Heat Transfer of Electrical MHD Non-Newtonian Fluid Over a Slendering Stretching Sheet

Gossaye Aliy[1,2] · **Naikoti Kishan**[2]

Abstract

In this paper, the problem of cross-diffusion and electric field effects on the MHD Williamson fluid flow across a variable thickness stretching sheet with flow slip is presented. The transformed differential equations are solved by using the optimal homotopy asymptotic method. Comparison of results has been made with the numerical solutions from the literature and an interesting covenant has been observed. Subsequently, the effects of governing parameters on the flow, heat and mass transfer characteristics of the problem are presented graphically and discussed exhaustively. Results reveal that velocity and temperature increase with an increase in the electric field. Finally, we observed that the Dufour and Soret numbers have drifted to control the thermal and concentration boundary layers.

Keywords OHAM · Soret · Dufour · Electric field · Slendering sheet · Viscous dissipation

List of Symbols

u, v	Velocity components in x and y directions
f	Dimensionless velocity
B	Magnetic field vector
K	Thermal conductivity
K_T	Thermal diffusion ratio
T_m	Mean fluid temperature
C_∞	Concentration of the fluid in the free stream
L_2^*	Dimensional temperature jump parameter
r_1	Maxwell's reflection coefficient
b	Physical parameter related to stretching sheet
m	Velocity power index parameter
M	Magnetic interaction parameter

✉ Gossaye Aliy
   gosyy610@gmail.com

1   Department of Mathematics, University of Gondar, Gondar, Ethiopia

2   Department of Mathematics, Osmania University, Hyderabad, India

g	Dimensionless temperature
Sc	Schmidt number
L_1	Dimensionless velocity slip parameter
L_3	Dimensionless concentration jump parameter
Nu_x	Local Nusselt number
Re_x	Local Reynolds number
C_p	Specific heat capacity
A	Coefficient related to stretching sheet
T	Temperature of the fluid
D_m	Molecular diffusivity
C	Concentration of the fluid
T_∞	Temperature of the fluid
L_1^*	Dimensional velocity slip parameter
L_3^*	Dimensional conc. jump parameter
a	Thermal accommodation coefficient
d	Concentration accommodation coeff
Pr	Prandtl number
Du	Dufour number
h	Dimensionless concentration
Sr	Soret number
L_2	Thermal slip parameter
C_f	Skin friction coefficient
Sh_x	Local Sherwood number

Greek Symbols

η	Similarity variable
σ	Electrical conductivity of the fluid
ρ	Density of the fluid
μ	Dynamic viscosity
ν	Kinematic viscosity
α	Wall thickness parameter
ξ_1	Mean free path (constant)
Γ	Positive characteristic time
Λ	Williamson fluid parameter

Introduction

Several researchers have attracted by the concept of heat and mass transfer as they have enormous applications in diverse disciplines such as classification of moisture and temperature among the farming fields and plantation of fruit trees. When mass and heat transfer happens at the same time, complex behavior was perceived in the connections between the guiding potentials and fluxes. And also, it is noticed that the energy flux can be furnished by both concentration and temperature gradients. The energy flux instigated by temperature gradient is known as the Soret effect and the energy flux activated by concentration gradient is named as the Dufour effect. These effects may be ignored as they are of less order in magnitude

when compared with the effects initiated by Fick's and Fourier's laws. But they have their own moment in the fields such as hydrology and geosciences.

The non-Newtonian fluids like Pseudoplastic fluids have lower viscosity when considered shear strain. Modern paints are examples of pseudoplastic materials. It is known that the Navier–Stokes equations are insufficient to show the physical properties of pseudoplastic fluids, hence there are some physical models were recommended to overcome this gap such as Ellis, Carreaus, Cross- and power law models.

The flow across a stretching sheet attracted several writers because of its enormous applications in several extents such as polymer extrusion, metallurgical processes, metal-spinning, and plastic films. A good example for the boundary layer flow over a stretching surface is the process of melt spinning (a technique used for rapid cooling of liquids) where the extrudate is stretched into a sheet when it is pulled from the die. Finally, when this sheet passes by the controlled cooling system, then it becomes solid.

Initially Eckert et al. [1] acknowledged the importance of Soret and Dufour effects and argued the consequence of these effects on heat transfer across a cylinder. Ybarra and Velarde [2] discussed the influence of Dufour and Soret on the stability of a binary gas layer heated from above or below. Later some progressive work is contributed to Dufour and Soret effects by considering various channels [3–6]. Further by viewing chemical reaction and magnetic field together with these effects, Postelnicu [7, 8] conferred a number of cases to study the qualities of mass and heat transfer in the convective fluid flow. He noted that raising the magnetic field reduces the Dufour and Soret values. Likewise, Alam and Rahman [9] have done the problem by considering MHD flow and Cheng [10, 11] argued the problem by assuming concentration, wall temperature, wall mass and wall heat fluxes as unchallengeable. Their one of significant results is an increase in Soret number causes to reduce the temperature and intensify the concentration field. Raju et al. [12]. discussed radiation and Soret effects on MHD nanofluid flow across a vertical moving plate through a porous medium and they observed that the Soret number and buoyancy parameter assist in raising the rate of heat transfer. Reddy and Sandeep [13] studied the heat and mass transfer of magnetic bio-convective flow caused by a rotating cone and plate in the presence of nonlinear thermal radiation and cross diffusion. Recently, Reddy et al. [14] investigated the effect of Cross Diffusion on Magneto-hydrodynamic Bio-Convection flow of Oldroyd-B nanofluid past a melting sheet and Reddy [15] studied the Cattaneo–Christov heat flux effect on hydromagnetic radiative Oldroyd-B liquid flow across a cone/wedge in the presence of cross-diffusion.

In non-Newtonian fluids, the most frequently encountered fluids are pseudoplastic fluids whose behavior has been explained by proposing different models like Carreaus model, Ellis model, Cross model, and Williamson fluid model. The behavior of blood flow is almost completely described by the Williamson model of non-Newtonian fluid. This model was proposed by Williamson [16] and later on used by several authors [17–20] to investigate fluid flow characteristics and obtain the solution of the governing system of equations by applying different methods. Gorla and Gireesha [21] worked on the Williamson nanofluid flow and heat transfer over a stretching/shrinking sheet with the convective boundary condition.

Lee [22] introduced the notion of variable thickness sheet by thin needles. Later, the work was continued on variable thickness surface by many researchers [23–26] and various physical effects on peristaltic transport of non- Newtonian fluids are examined by the researchers [27, 28]. Peristaltic transport of Johnson-Segalman and Williamson fluids with slip Hina et al. [29]. and without slip Iftikhar et al. [30]. conditions are respectively studied.

Researchers studied the perturbation techniques to get the solution of strongly nonlinear combined problems. These methods collect and group small parameters which cannot be found easily. The methods like Artificial Parameters Method Arshad et al. [31]., Homo-

topy Analysis Method (HAM) Liu [32] and Homotopy Perturbation Method (HPM) Hayat et al. [33]. were introduced for the small parameter. The above analytic methods joined the homotopy with the perturbation techniques.

OHAM is a semi-analytical technique that is directed forward to apply on different type of problems and the existence of any small or large parameters are not significant. Marinca et al. [34]. was initially introduced the basic concept of this method in 2008. OHAM reduces the extent of the computational domain. It is a reliable analytical technique and has already been successfully applied to various nonlinear coupled differential equations occurring in science, engineering and other fields of studies. Marinca and Herisanu applied OHAM on different problem (see, [35–37]). Many researchers applied OHAM to study fluid flow problems [38–41]. Recently, Gossaye and Kishan [42, 43] apply the optimal homotopy asymptotic method to the electrical MHD non-Newtonian fluid flows over a stretching sheet.

In this paper, we studied the heat and mass transfer characteristics of Dufour and Soret effects on electrical MHD Williamson fluid flow over a stretching surface with flow slip and variable thickness using OHAM. To the author's utmost knowledge, so far no writing has conveyed these types of investigation. The momentum, energy and concentration equations are reduced into a set of the system of ODEs and then solved by using an effective analytical technique OHAM. The influence of dissimilar governing parameters on the velocity, temperature and concentration profiles is examined using graphs and tables.

Mathematical Formulation

Consider an electrical MHD two-dimensional steady laminar flow of Williamson fluid past a slandering stretching sheet coinciding with the plane $y = 0$ as portrayed in Fig. 1. The origin is positioned at a slit through which the surface is drawn through the fluid medium. Assume that

$$y = A(b + x)^{\frac{-m+1}{2}}, \quad U_w = U_0(b + x)^m, \quad v_w = 0, m \neq 1$$
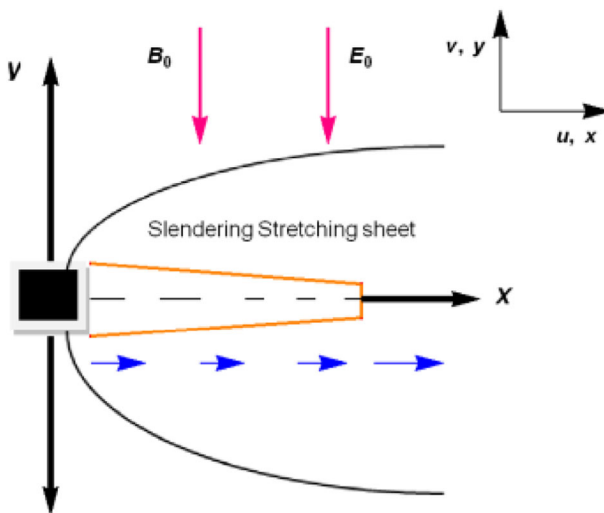

Fig. 1 Flow configuration and co-ordinate system

with the presence of an external electric field and the sheet is sufficiently thin and m is the velocity power index.

As the fluid is electrically conducting and in the existence of an external electric field, the Lorenz force is given by $J \times B$, where $J = \sigma(E + V \times B)$ is the Joule current, σ is the electrical conductivity, $V = (u, v)$ is the fluid velocity, $B = (0, B_0, 0)$ and $E = (0, 0, -E_0)$ are the transverse magnetic and electric field vectors, respectively. The magnetic and electric fields are applied perpendicular to the flow, such that the Reynolds number is selected small. The applied magnetic field is greater when it is compared to the induced magnetic field. Hence the induced magnetic field is negligible for small magnetic Reynolds number.

The coordinate system is illustrated in Fig. 1 above. The Cauchy stress tensor S for Williamson fluid model is written as (Dapra and Searpi [44]):

$$S = -pI + \tau_1 \tag{1}$$

$$\tau_1 = \left(\mu_\infty + \frac{\mu_0 - \mu_\infty}{1 - \gamma_1 \Gamma} \right) A_1, \tag{2}$$

where μ_0 and μ_∞ are the limiting viscosity at 0 and at infinity shear rate, τ_1 is the extra stress tensor, I is an identity tensor, $\Gamma > 0$ is a time constant, A_1 is the first Rivlin–Erickson tensor and the shear rate γ_1 is written as:

$$\gamma_1 = \sqrt{0.5\pi} \text{ and } \pi = trace(A_1^2), \tag{3}$$

where π is the second invariant strain tensor. Here we considered the case for which $\mu_\infty = 0$ and $\gamma_1 \Gamma < 1$. Hence, τ_1 is defined as

$$\tau_1 = \left(\frac{-\mu_0}{\gamma_1 \Gamma - 1} \right) A_1. \tag{4}$$

By using the binomial expansion, we obtain

$$\tau_1 = \mu_0(1 - \gamma_1 \Gamma) A_1. \tag{5}$$

The conservative equations in the aforementioned conditions for the Williamson fluid flow with the slip boundary conditions are given as (see, [45–47])

Continuity equation

$$\frac{\partial u}{\partial x} + \frac{\partial v}{\partial y} = 0. \tag{6}$$

Momentum equation

$$u \frac{\partial u}{\partial x} + v \frac{\partial u}{\partial y} = v \frac{\partial^2 u}{\partial y^2} + \Gamma v \sqrt{2} \left(\frac{\partial u}{\partial y} \right) \left(\frac{\partial^2 u}{\partial y^2} \right) + \frac{1}{\rho} \left(\nabla \times \frac{B}{\mu_0} \right) \times B. \tag{7}$$

Taking the last term and applying the equation of electrodynamic $\nabla \times B = J\mu_0$, where μ_0 is the magnetic permeability, we have

$$\frac{1}{\rho} \left(\nabla \times \frac{B}{\mu_0} \right) \times B = \frac{J \times B}{\rho} = \frac{1}{\rho}(J \times B) = \frac{1}{\rho}(\sigma(E + V \times B) \times B)$$

$$= \frac{1}{\rho}(\sigma((0, 0, -E_0) + (u, v, 0) \times (0, B_0, 0)) \times (0, B_0, 0))$$

$$= \frac{1}{\rho}(\sigma(0, 0, -E_0 + uB_0) \times (0, B_0, 0))$$

$$= \frac{1}{\rho}(\sigma(-(-E_0 + uB_0)B_0) = \frac{\sigma}{\rho}\left(B_0 E_0 - uB_0^2 \right)$$

$$= -\frac{\sigma B_0^2}{\rho} u + \frac{\sigma}{\rho} B_0 E_0 \tag{8}$$

Hence we can write Eq. (7) as

$$u\frac{\partial u}{\partial x} + v\frac{\partial u}{\partial y} = v\frac{\partial^2 u}{\partial y^2} + \Gamma v\left(\frac{\partial u}{\partial y}\right)\left(\frac{\partial^2 u}{\partial y^2}\right)\sqrt{2} - u\frac{\sigma B_0^2}{\rho} + \frac{\sigma}{\rho} B_0 E_0. \tag{9}$$

Energy equation

$$u\frac{\partial T}{\partial x} + v\frac{\partial T}{\partial y} = \left(\frac{k}{\rho C_p}\right)\left(\frac{\partial^2 T}{\partial y^2}\right) + \frac{D_m k_T}{C_p C_s}\frac{\partial^2 T}{\partial y^2} + \frac{\mu}{\rho C_p}\left(\frac{\partial u}{\partial y}\right)^2$$
$$+ \frac{1}{\rho C_p}\left(\frac{1}{\sigma}\left(\nabla \times \frac{B}{\mu_0}\right).\left(\nabla \times \frac{B}{\mu_0}\right)\right). \tag{10}$$

Taking the last term and applying the equation of electrodynamic $\nabla \times B = J\mu_0$, where μ_0 is the magnetic permeability, we have

$$\frac{1}{\rho C_p}\left(\frac{1}{\sigma}\left(\nabla \times \frac{B}{\mu_0}\right).\left(\nabla \times \frac{B}{\mu_0}\right)\right) = \frac{1}{\rho C_p}\frac{1}{\sigma}(J.J)$$
$$= \frac{\sigma}{\rho C_p}((E + V \times B).(E + V \times B))$$
$$= \frac{\sigma}{\rho C_p}\left((-E_0 + uB_0)\hat{k}.(-E_0 + uB_0)\hat{k}\right)$$
$$= \frac{\sigma}{\rho C_p}(-E_0 + uB_0)^2 = \frac{\sigma}{\rho C_p}(uB_0 - E_0)^2. \tag{11}$$

Hence Eq. (10) can be written as

$$u\frac{\partial T}{\partial x} + v\frac{\partial T}{\partial y} = \left(\frac{k}{\rho C_p}\right)\left(\frac{\partial^2 T}{\partial y^2}\right) + \left(\frac{D_m k_T}{C_p C_s}\right)\left(\frac{\partial^2 C}{\partial y^2}\right) + \left(\frac{\partial u}{\partial y}\right)^2\left(\frac{\mu}{\rho C_p}\right) + \frac{\sigma}{\rho C_p}(uB_0 - E_0)^2. \tag{12}$$

Concentration equation

$$u\frac{\partial C}{\partial x} + v\frac{\partial C}{\partial y} = D_m\left(\frac{\partial^2 C}{\partial y^2}\right) + \left(\frac{D_m k_T}{T_m}\right)\left(\frac{\partial^2 T}{\partial y^2}\right) \tag{13}$$

with the corresponding boundary conditions

$$\begin{cases} u(x, y) = U_w(x) + L_1^*\left(\frac{\partial u}{\partial y}\right), v(x, y) = 0, \\ T(x, y) = T_w(x) + L_2^*\left(\frac{\partial T}{\partial y}\right), C(x, y) = C_w(x) + L_3^*\left(\frac{\partial C}{\partial y}\right), \\ u \to 0, T \to T_\infty, C \to C_\infty \text{ as } y \to \infty, \end{cases} \tag{14}$$

where

$$L_1^* = \xi_1(x + b)^{\frac{1-m}{2}}\left(\frac{2}{r_1} - 1\right), \quad \xi_2 = \frac{\xi_1}{Pr}\left(\frac{2\gamma}{1 + \gamma}\right),$$

$$L_2^* = \xi_2(x + b)^{\frac{1-m}{2}}\left(\frac{2}{a} - 1\right), \quad \xi_3 = \frac{\xi_2}{Pr}\left(\frac{2\gamma}{1 + \gamma}\right),$$

$$L_3^* = \xi_3(x + b)^{\frac{1-m}{2}}\left(\frac{2}{d} - 1\right), \quad B(x) = B_0(x + b)^{\frac{1-m}{2}},$$

$$T_w(x) = T_\infty + T_0(x + b)^{\frac{1-m}{2}} \text{ and } C_w(x) = C_\infty + C_0(x + b)^{\frac{1-m}{2}}.$$

Int. J. Appl. Comput. Math (2019) 5:80

Page 7 of 22   80

To change the governing equations into a set of nonlinear ODEs, we establish the following similarity transformations:

$$
\begin{cases}
\psi(x, y) = f(\eta)\sqrt{\dfrac{2\nu U_0(x+b)^{m+1}}{1+m}}, \, \eta = y\sqrt{\dfrac{(m+1)U_0(x+b)^{-1+m}}{2\nu}} \\
g = \dfrac{T-T_\infty}{T_w-T_\infty} \text{ and } h = \dfrac{C-C_\infty}{C_w-C_\infty}.
\end{cases}
\tag{15}
$$

If stream function ψ is defined as $u = \frac{\partial \psi}{\partial y}$ and $v = -\frac{\partial \psi}{\partial x}$, then u and v satisfy Eq. (6) and become

$$
u = f'(\eta)U_0(b+x)^m \text{ and } v = -\sqrt{\frac{(m+1)\nu U_0(x+b)^{m-1}}{2}}\left(f(\eta) + \eta f'(\eta)\left(\frac{m-1}{m+1}\right)\right).
\tag{16}
$$

After a long simplification with the help of Eqs. (15) and (16) the transformed momentum, energy and concentration Eqs. (6), (9) and (13) along with the boundary conditions (14) are given by:

$$
f''' + f''(\Lambda f''' + f) + M(E_1 - f') - 2\left(\frac{m(f')^2}{m+1}\right) = 0
\tag{17}
$$

$$
g'' + Pr\left(\frac{m-1}{m+1}gf' + g'f + h''Du + (f'')^2 Ec + (f' - E_1)^2 MEc\right) = 0
\tag{18}
$$

$$
h'' + \left(\frac{m-1}{m+1}hf' + fh' + g''Sr\right)Sc = 0.
\tag{19}
$$

The corresponding boundary conditions are

$$
\begin{cases}
f(0) = \alpha\left(\frac{1-m}{m+1}\right)\left[1 + L_1 f''(0)\right], \, f'(0) = 1 + L_1 f''(0), \, g(0) = 1 + L_2 g'(0), \\
h(0) = 1 + L_3 h'(0), \, f'(\eta) \to 0, \, g(\eta) \to 0, h(\eta) \to 0, \text{ as } \eta \to \infty
\end{cases}
\tag{20}
$$

where $\Lambda, M, Pr, Du, Sc, Sr, E_1$ and Ec are defined as

$$
\Lambda = \Gamma\sqrt{\frac{(m+1)U_0^3(x+b)^{3m-1}}{\nu}}, \quad M = 2\frac{\sigma B_0^2}{\rho U_0(m+1)},
$$

$$
Pr = \mu\frac{C_p}{k}, \, Du = D_m k_T \frac{(C_w - C_\infty)}{\nu C_p C_s(T - T_\infty)}, \quad Sc = \frac{\nu}{D_m},
$$

$$
Sr = D_m k_T \frac{(T_w - T_\infty)}{\nu T_m(C_w - C_\infty)}, \quad E_1 = \frac{E_0}{U_w B_0(x+b)^m}, \quad Ec = \frac{U_w^2}{C_p(T_w - T_\infty)}.
$$

The skin-friction coefficient C_f, local Nusselt number Nu_x and local Sherwood number Sh_x are defined as

$$
C_f = 2\mu\frac{\partial u}{\partial y}\frac{1}{\rho U_w^2}, \, Nu_x = \frac{\partial T}{\partial y}\frac{(b+x)}{T_w - T_\infty}, \, Sh_x = \frac{\partial C}{\partial y}\frac{(d+x)}{C_w - C_\infty}
\tag{21}
$$

By using Eq. (14), Eq. (21) becomes

$$
\sqrt{Re_x}C_f = 2\sqrt{\frac{1+m}{2}}f''(0), \quad Nu_x = -\sqrt{\frac{1+m}{2}}\sqrt{Re_x}g'(0) \text{ and } Sh_x = -\sqrt{\frac{1+m}{2}}\sqrt{Re_x}h'(0),
$$

where $Re_x = \frac{X U_w}{\nu}$ and $X = (b+x)$.

Analytical Solution Using OHAM

The OHAM is now applied to nonlinear ODEs (17)–(19) along with the boundary condition (20) by considering the following assumptions

$$f = f_0 + pf_1 + p^2 f_2, \ g = g_0 + pg_1 + p^2 g_2, \ h = h_0 + ph_1 + p^2 h_2,$$

$$H_1(p) = C_1 p + C_2 p^2, \ H_2(p) = C_3 p + C_4 p^2, \ H_3(p) = C_5 p + C_6 p^2,$$

where $p \in [0, 1]$ is an embedding parameter, $H_j(p)$, $j = 1, 2, 3$ is an auxiliary function different from zero, and C_i, $(i = 1, 2, 3, 4, 5, 6)$ are convergence parameters [34, 48]).

Analytical Solution of the Momentum Boundary Layer Problem

The OHAM is applied to Eq. (17) using the following assumption

$$L = f'' + f''' \text{ and}$$

$$N = f'''(1 + \Lambda f'') + f f'' + M(E_1 - f') - \left(\frac{2m}{m+1}\right)(f')^2 - (f'' + f'''), \quad (22)$$

where L and N are the linear and nonlinear operators, respectively. Hence, the OHAM family of the equation is given by

$$(1 - p)(f'' + f''') = H_1(p)\begin{bmatrix} f''' + \Lambda f'' f''' + f'' f \\ +M(E_1 - f') - \left(\frac{2m}{m+1}\right)(f')^2 \end{bmatrix}. \quad (23)$$

After simplification, equating the same powers of $p -$ terms and using the boundary conditions (20), we have the following:

Equating the zero order equation p^0, we obtain

$$f_0' + f_0''' = 0 \quad f_0(0) = \alpha \left(\frac{1-m}{m+1}\right)[1 + L_1 f'''(0)], \quad f_0'(0) = 1 + L_1 f_0''(0). \quad (24)$$

Equating the first order equation p^1, we obtain

$$f_1'' + f_1''' = f_0''' + f_0'' + C_1 \begin{bmatrix} f_0''' + \Lambda f_0'' f_0''' - \left(\frac{2m}{m+1}\right) f_0'^2 \\ -M f_0' + M E_1 + f_0 f_0'' \end{bmatrix}, \quad (25)$$

$$f_1(0) = \alpha \left(\frac{1-m}{m+1}\right) f_1''(0), \ f_1'(0) = 0.$$

Equating the second order equation p^2, we obtain

$$f_2'' + f_2''' = f_1''' + f_1'' + C_1 \begin{bmatrix} f_1''' + f_0 f_1'' + f_1 f_0'' - \left(\frac{4m}{m+1}\right) f_0' f_1' \\ -M f_1' + M E_1 + \Lambda \left[f_1'' f_0''' + f_0'' f_1'''\right] \end{bmatrix}$$

$$+ C_2 \begin{bmatrix} f_0''' + \Lambda f_0'' f_0''' - \left(\frac{2m}{m+1}\right) f_0'^2 \\ -M f_0' + M E_1 + f_0 f_0'' \end{bmatrix}, \quad (26)$$

$$f_2(0) = \alpha \left(\frac{1-m}{m+1}\right) f_2''(0), \quad f_2'(0) = 0.$$

After solving the ordinary differential Eqs. (24)–(26) with the corresponding boundary conditions, we obtain

$$f_0 = -\frac{e^{-\eta}(1 - e^\eta + m - e^\eta m - e^\eta \alpha - 2e^\eta L_1 \alpha + e^\eta m\alpha + 2e^\eta L_1 m\alpha)}{(1 + L_1)(1 + m)} \quad (27)$$

The other two terms f_1 and f_2 are too large to mention here. Hence, the solution f $(\eta, C_i), i = 1, 2$ is given by:

$$f(\eta, C_i) = f_0(\eta) + f_1(\eta, C_1, C_2) + f_2(\eta, C_1, C_2). \tag{28}$$

To find the constants C_1 and C_2, we use the residual equation for the problem obtained in the form

$$R_1(\eta, C_1, C_2) = \begin{bmatrix} f''' + \Lambda f'' f''' + f f'' \\ +M(E_1 - f') - \left(\frac{2m}{m+1}\right)(f')^2 \end{bmatrix}. \tag{29}$$

The unknown convergence parameters C_1 and C_2 can be optimally obtained from the following conditions given below

$$\frac{\partial J_1(C_1, C_2)}{\partial C_1} = \frac{\partial J_1(C_1, C_2)}{\partial C_2} = 0, \quad \text{where } J_1(C_i) = \int_0^5 R_1^2(\eta, C_i)d\eta. \tag{30}$$

In the particular case when $m = 0.5, E_1 = 0.01, L_1 = \Lambda = M = 0.1$ and $\alpha = 1$, the values of the convergence parameters are given by

$$C_1 = 0.20915340986446768, \quad C_2 = 0.5446628379971291$$

After substituting all the parameters, we get

$$f(\eta) = -0.606060606060606 e^{-\eta}\left(1.5 - 2.1e^{\eta}\right)$$

$$+ 0.1836547291092745 e^{-2\eta}\begin{pmatrix} 0.10980554017884556 + 0.16741580115896e^{\eta} \\ -0.3322673815129e^{2\eta} + 0.3858880411999e^{\eta}\eta \\ +0.001138840316783e^{2\eta}\eta \end{pmatrix}$$

$$+ 0.01855098273831 e^{-3\eta}\begin{pmatrix} -0.03904254535570611 + 0.081522371635994e^{\eta} \\ +4.61119455329911e^{2\eta} - 6.195930191621276e^{3\eta} \\ -0.16949057925006e^{\eta}\eta + 4.79747772755256e^{2\eta}\eta \\ +0.0291245122014e^{3\eta}\eta - 0.14783771483123e^{2\eta}\eta^2 \end{pmatrix} \tag{31}$$

Analytical Solution of the Thermal Boundary Layer Problems

The OHAM is applied to nonlinear ODE (18) using the following assumption

$$L = g + g' \text{ and}$$

$$N = g'' + Pr\begin{pmatrix} \frac{m-1}{m+1}gf' + g'f + h''Du \\ +(f'')^2 Ec + MEc(f' - E_1)^2 \end{pmatrix} - (g' + g), \tag{32}$$

where L and N are the linear and nonlinear operators, respectively. Therefore the OHAM family equation is given by

$$(1 - p)(g' + g) = H_2(p)\left[g'' + Pr\begin{pmatrix} \frac{m-1}{m+1}f'g + fg' + Duh'' \\ +Ec(f'')^2 + MEc(f' - E_1)^2 \end{pmatrix}\right]. \tag{33}$$

After simplification, equating the like powers of p-terms and using the boundary conditions (20), we have the following:

Equating the zero order equation p^0, we get

$$g_0' + g_0 = 0, \quad g_0(0) = 1 + L_2 g_0'(0) \tag{34}$$

Equating the first order equation p^1, we get

$$g_1' + g_1 = g_0' + g_0 + C_3 \left[g_0'' + Pr \left(\begin{matrix} \frac{m-1}{m+1} f_0' g_0 + f_0 g_0' + Duh_0'' \\ + \left(Ec\left(f_0''\right)^2 + MEc\left(f_0' - E_1\right)^2 \right) \end{matrix} \right) \right] \tag{35}$$

$$g_1(0) = L_2 g_1'(0).$$

Equating the second order equation p^2, we get

$$g_2' + g_2 = g_1' + g_1 + C_3 \left[g_1'' + Pr \left(\begin{matrix} +f_1 g_0' + \frac{m-1}{m+1} f_0' g_1 + \frac{m-1}{m+1} f_1' g_0 + f_0 g_1' \\ + Duh_1'' + \left(2Ecf_0'' f_1'' + MEc\left(f_1' - E_1\right)^2 \right) \end{matrix} \right) \right]$$
$$+ C_4 \left[g_0'' + Pr \left(\begin{matrix} \frac{m-1}{m+1} f_0' g_0 + f_0 g_0' + Duh_0'' \\ + \left(Ec\left(f_0''\right)^2 + MEc\left(f_0' - E_1\right)^2 \right) \end{matrix} \right) \right], \tag{36}$$

$$g_2(0) = L_2 g_2'(0).$$

After solving the ODEs (34)–(36) with the corresponding boundary conditions, we obtain

$$g_0 = \frac{e^{-\eta}}{1 + L_2}. \tag{37}$$

The other terms g_1 and g_2 are very large to mention here. Hence, the solution $g(\eta, C_i), i = 1, 2, \ldots, 6$ is given by:

$$g(\eta, C_i) = g_0(\eta) + g_1(\eta, C_i) + g_2(\eta, C_i). \tag{38}$$

The residual equation for the problem obtained in the form

$$R_2(\eta, C_i) = g'' + Pr \left(\begin{matrix} \frac{m-1}{m+1} f'g + fg' + Duh'' \\ + Ec\left(f''\right)^2 + MEc\left(f' - E_1\right)^2 \end{matrix} \right). \tag{39}$$

The unknown convergence parameters C_i can be optimally identified from the following conditions given below

$$\frac{\partial J_2(C_i)}{\partial C_1} = \frac{\partial J_2(C_i)}{\partial C_2} = \frac{\partial J_2(C_i)}{\partial C_3} = \frac{\partial J_2(C_i)}{\partial C_4} = \frac{\partial J_2(C_i)}{\partial C_5} = \frac{\partial J_2(C_3, C_4)}{\partial C_6} = 0,$$

where $J_2(C_i) = \int_0^5 R_2^2(\eta, C_i) d\eta.$ \tag{40}

After obtaining the convergence parameters the simplified solution will be given by

$$g(\eta, C_i) = g_0(\eta) + g_1(\eta, C_i) + g_2(\eta, C_i). \tag{41}$$

In the particular case when $m = 0.5$, $Du = Ec = Sc = 0.2$, $E_1 = 0$, $Sr = Pr = Le = 2$, $\Lambda = M = L_1 = L_2 = L_1 = 0.1$, then the results of the convergence parameters are given by

$C_1 = 0.207433880957080,$ $C_2 = 0.5521142384261435,$ $C_3 = -0.4353462064643$
$C_4 = 1.417403883169999,$ $C_5 = -0.4414273478882194,$ $C_6 = 2.01605498183113$

Int. J. Appl. Comput. Math (2019) 5:80

Page 11 of 22   **80**

Hence the approximate analytical solution can be expressed as

$$
g(\eta) = 2.7276429222215e^{-\eta} + 0.4139475487061e^{-2\eta} \begin{pmatrix} 1.541325830138718 \\ -1.58188703619499e^{\eta} \\ +1.0951525635196e^{\eta}\eta \end{pmatrix}
$$

$$
+ 0.041812883707687e^{-\eta} \begin{pmatrix} 0. + 9.68401158814421e^{-2\eta} - 40.92663701745\eta \\ + e^{-\eta}(-53.41574223550 + 4.2487405429854\eta) \\ + 4.604486409775797\eta^2 \end{pmatrix}
$$

$$(42)$$

Analytical Solution of the Concentration Boundary Layer Problems

The OHAM is applied to Eq. (19) under the following assumption

$$
L = h' + h \quad \text{and} \quad N = h'' + Sc\left(\frac{m-1}{m+1}hf' + h'f + Srg''\right) - (h' + h), \tag{43}
$$

where L and N are the linear and nonlinear operators, respectively. Therefore the OHAM family equation is given by

$$
(1-p)(h'+h) = H_3(p)\left[h'' + Sc\left(\frac{m-1}{m+1}f'h + fh' + Srg''\right)\right]. \tag{44}
$$

After simplification, equating the like powers of p-terms and using the boundary condition (20), we have the following:

Equating the zero order equation p^0, we get

$$
h_0' + h = 0, \quad h_0(0) = 1 + L_3h_0'(0) \tag{45}
$$

Equating the first order equation p^1, we get

$$
h_1' + h_1 = h_0' + h_0 + C_5\left[h_0'' + Sc\left(\begin{matrix}\frac{m-1}{m+1}f_0'^{h_0} \\ +f_0h_0' + Srg_0''\end{matrix}\right)\right], \quad h_1(0) = L_3h_2'(0). \tag{46}
$$

Equating the second order equation p^2, we get

$$
h_2' + h_2 = h_1' + h_1 + C_5\left[h_1'' + Sc\left(\begin{matrix}\frac{m-1}{m+1}f_1'h_0 + \frac{m-1}{m+1}f_0'h_1 \\ +f_1h_0' + f_0h_1' + Srg_1''\end{matrix}\right)\right]
$$

$$
+ C_6\left[h_0'' + Sc\left(\begin{matrix}\frac{m-1}{m+1}f_0'^{h_0} \\ +f_0h_0' + Srg_0''\end{matrix}\right)\right], h_2(0) = L_3h_2'(0). \tag{47}
$$

After solving the ODEs (45)–(47) with the corresponding boundary conditions, we obtain

$$
h_0 = \frac{e^{-\eta}}{1 + L_3}. \tag{48}
$$

The terms h_1 and h_2 are too large to mention here. Hence, the solution $h(\eta, C_i), i = 1, 2, \ldots, 6$ is given by:

$$
h(\eta, C_i) = h_0(\eta) + h_1(\eta, C_i) + h_2(\eta, C_i). \tag{49}
$$

The residual equation for the problem obtained in the form

$$
R_3(\eta, C_i) = h'' + Sc\left(\frac{m-1}{m+1}f'h + fh' + Srg''\right). \tag{50}
$$

Table 1 Comparison of the values of $-f''(0)$ when $M = \Lambda = E_1 = L_1 = 0$, $\alpha = 0.5$.

m	Khader and Megahed [49]	Fang et al. [50]	Present result
0.5	0.9798	0.9799	0.97901
1	1.0000	1.0000	1.00000
2	1.0234	1.0234	1.02375
3	1.0358	1.0359	1.03665
5	1.0486	1.0486	1.04987
7	1.0551	1.0550	1.05654
9	1.0588	1.0589	1.05955
10	1.0603	1.0603	1.06201

The unknown convergence parameters C_i can be optimally identified from the following conditions:

$$\frac{\partial J_3(C_i)}{\partial C_1} = \frac{\partial J_3(C_i)}{\partial C_2} = \frac{\partial J_3(C_i)}{\partial C_3} = \frac{\partial J_3(C_i)}{\partial C_4} = \frac{\partial J_3(C_i)}{\partial C_5} = \frac{\partial J_3(C_i)}{\partial C_6} = 0, \qquad (51)$$

where $J_3(C_i) = \int_0^5 R_3^2(\eta, C_i)d\eta$.

After obtaining the convergence parameters the simplified solution will be given by

$$h(\eta) = h_0(\eta) + h_1(\eta) + h_2(\eta). \qquad (52)$$

In the particular case when $m = 0.5$, $Du = Ec = Sc = 0.2$, $E_1 = 0$, $Sr = Pr = Le = 2$, $\Lambda = M = L_1 = L_2 = L_1 = 0.1$, then the results of the convergence parameters are given by

$C_1 = 0.207433880957080$, $C_2 = 0.5521142384261435$, $C_3 = -0.4353462064643$
$C_4 = 1.417403883169999$, $C_5 = -0.4414273478882194$, $C_6 = 2.01605498183113$

Hence the approximate analytical solution can be expressed as

$$h(\eta) = 0.689113522052e^{-\eta} + 0.166958844644e^{-2\eta} \begin{pmatrix} 0.2913420496062248 \\ -2.32102499519625e^{\eta} \\ -2.7531823687788e^{\eta}\eta \end{pmatrix}$$

$$+ 0.045994172078455e^{-\eta} \begin{pmatrix} +e^{-\eta}(7.3134074370858 - 0.616512685057\eta) \\ +36.611365444964\eta + 0.77416695326706\eta^2 \\ 0.06491669864885e^{-2\eta} \end{pmatrix} \quad (53)$$

To check the validity of the analytical method (OHAM) used in this study, we compared the results for $-f''(0)$ with the previously published result, see Table 1.

Result and Discussion

The group of nonlinear ODEs (17)–(19) subject to the restrictions (20) is solved analytically by employing the OHAM. We make known the results to keep up the effect of numerous parameters such as electric field, Soret, Dufour, and others on the three usual profiles (velocity, temperature and concentration). Also, we examined the skin friction coefficient with the aid
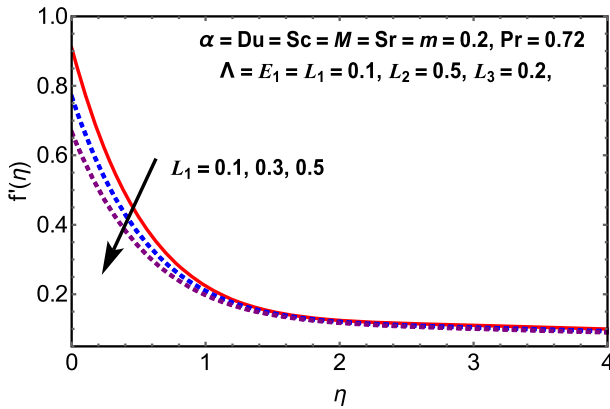
Fig. 2 Effects of velocity slip parameter L_1 on dimensionless velocity
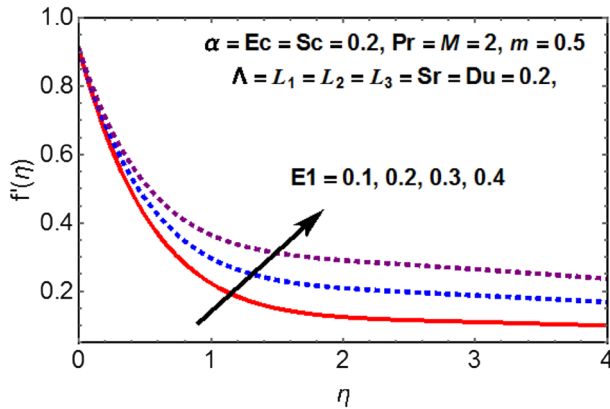

Fig. 3 Effect of electric field E_1 on dimensionless velocity

of a table. Table 1 is computed to validate the present analytic solution in a limiting case. It is observed that the present limiting results have a good match with the previously published results.

Hydrodynamic Results

Figures 2, 3, 4 and 5 exhibit the dimensionless velocity profile $f'(\eta)$ for dissimilar values of velocity slip parameter L_1, electric field parameter E_1 and magnetic field parameter M. From Fig. 2 we have seen that the rise in velocity slip parameter declines the velocity. The velocity of the flow is reduced by the slip parameter near the sheet. Influence of electrical field parameter in the velocity field portrayed in Fig. 3. As the value of electric field parameter rises, the velocity increases nearer to the stretching sheet. It is the fact that, the Lorentz force increasing as a result of electric field acts as an accelerating force reduces the frictional resistance which causes to change the streamlines far from the stretching plate.

The influence of magnetic field parameter M on the velocity profiles in the absence and presence of electric field, respectively, is depicted in Figs. 4 and 5, respectively. Figure 4 demonstrates the impact of M on the velocity profile in the absence of an electric field
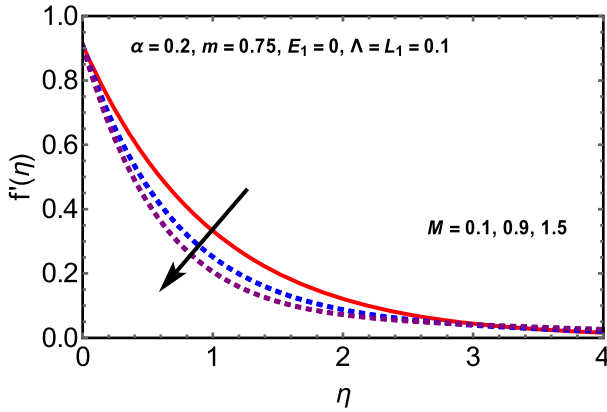
Fig. 4 Effect of M on dimensionless velocity with the absence of electric field
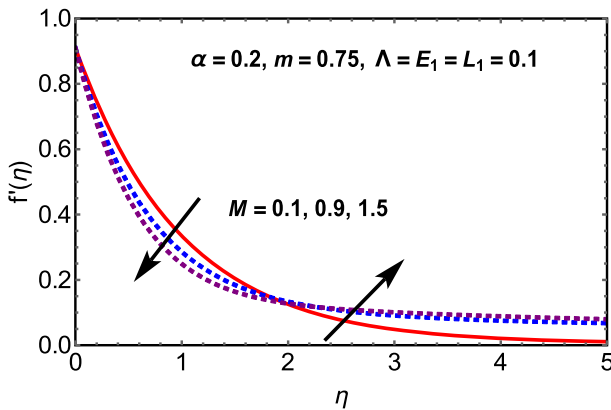

Fig. 5 Effect of M on dimensionless velocity with the presence of electric field

$(E_1 = 0)$. The velocity field reduces significantly with an increase in the values of M. It is obvious that the magnetic field depends on the Lorenz force, which is stronger for a larger magnetic field. Because of the absence of an electric field, the Lorenz force increases the frictional force, which performs as a retarding force that opposes the Williamson fluid flow. Figure 5 reveals that in the existence of an electric field $(E_1 \neq 0)$, as the magnetic field parameter M increases, the velocity boundary layer decreases. After some value of η away from the wall, it increases significantly over the stretching sheet. Due to an electric field which acts as speeding up the body force, accelerate the Williamson fluid flow.

Thermal Results

Effects of velocity slip parameter L_1, thermal slip parameter L_2, electric field parameter E_1, Dufour number Du, Eckert number Ec and Soret number Sr are revealed in the Figs. 6, 7, 8, 9 and 10. From Fig. 6 we observed that the rise in L_1 boost up the temperature profiles. The velocity of the flow is vital to disperse the temperature of the sheet. This, in turn, intensifies the temperature. Generally, raising the slip causes to boost up the wall friction and leads to
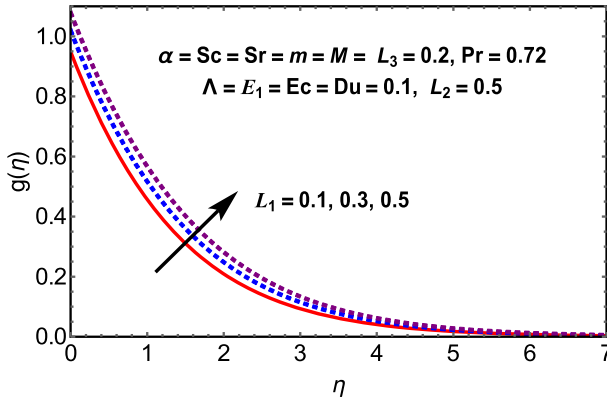
Fig. 6 Effects of velocity slip parameter L_1 on dimensionless temperature
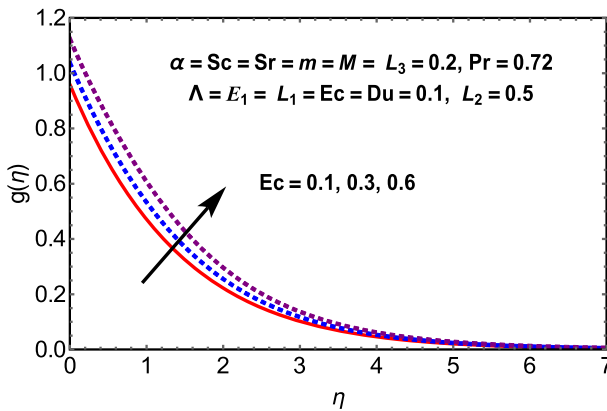

Fig. 7 Effect of viscous dissipation parameter Ec on dimensionless temperature

produce additional heat to the flow. Figure 7 demonstrates the impact of Ec. It is seen that the rise in Ec, speed up the temperature distribution and hence increase the thermal boundary layer thickness. This leads to the decline of the rate of heat transfer from the plate sheet.

Figure 8 shows that the effect of thermal slip parameter L_2 the temperature field g(η). It is observed that the temperature decreases with the rise in L_2. However, the increase in thermal jump parameter raises the thermal accommodation coefficient. This can lead to reducing the thermal diffusion toward the flow. On account of this, the temperature boundary layer also gets thinner and it is known that the Newtonian fluid occupies lower temperature field compared with non-Newtonian fluid. Dufour and Soret effects on the temperature profiles are revealed in Figs. 9 and 10, respectively. The values of the Soret and Dufour numbers are selected deliberately that their product is constantly providing the mean temperature T_m is kept constant as well. With an increase in the Dufour number and a decrease in Soret number, the temperature difference between hot and surrounding fluid reduces, which in result heightens the temperature.
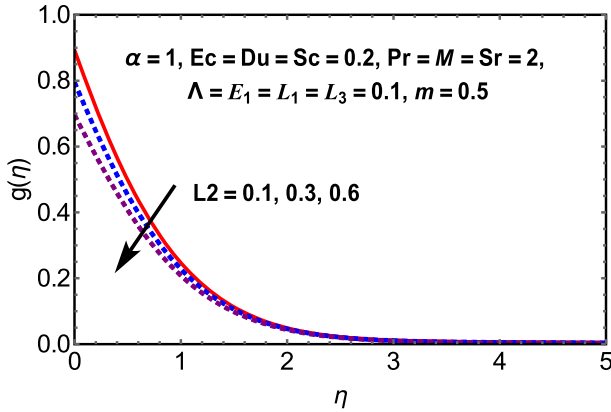
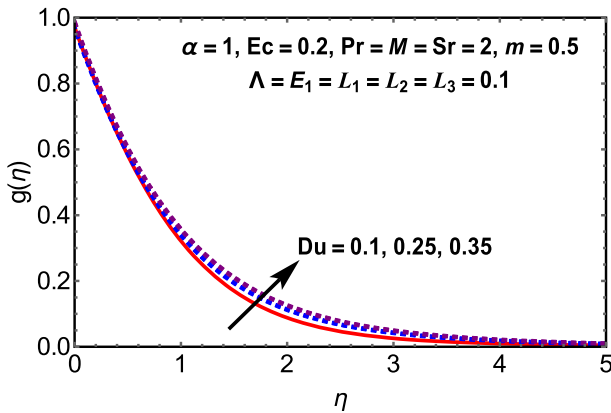**Fig. 8** Effect of thermal slip parameter L_2 on dimensionless temperature

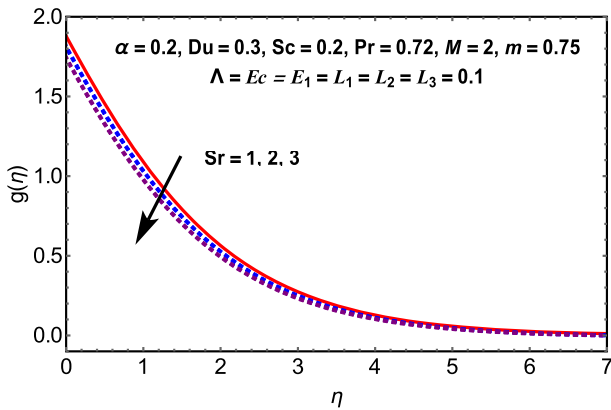**Fig. 9** Effect of Dufour number Du on dimensionless temperature

Fig. 10 Effect of Soret number Sr on dimensionless temperature

Concentration Results

Figures 11, 12, 13, 14 and 15 illustrate the effects of Eckert number Ec, thermal and concentration parameters L_2 and L_3, respectively, Soret Sr and Dufour Du numbers. Figure 11 demonstrates that as the Eckert number Ec increases, the concentration decreases up to some point away from the wall and then become increases significantly. Figures 12 and 13 display that the impact of thermal and concentration slip parameters on concentration field, respectively. It is seen that the concentration profile reduced with the rise in thermal and concentration slip parameters, respectively.

Figures 14 and 15 depict Soret and Dufour effects on concentration profiles, respectively. With a decrease in a Soret and a Dufour number, the temperature difference between hot and surrounding fluid declines, which in result increases the temperature distribution. Further, the intermolecular forces become weak and, consequently, the concentration diminutions.

The variations of Nusselt and Sherwood numbers with Dufour and Soret numbers for different values of thermal and concentration slip parameters are shown in Figs. 16 and 17, respectively. Figure 16 shows that the Nusselt number decreases for increasing values of thermal slip parameter. However, it is increasing for the rising values of Dufour number Du.
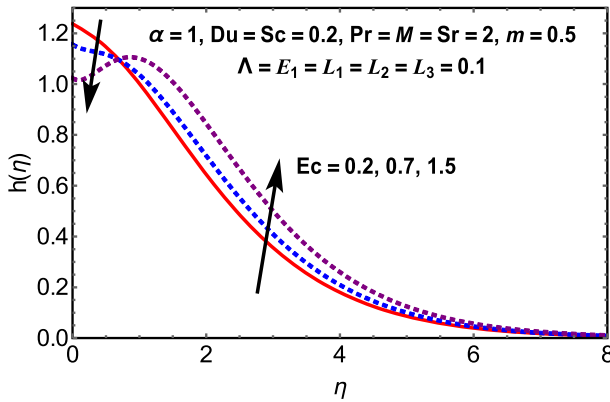

Fig. 11 Effect of viscous dissipation parameter Ec on dimensionless concentration
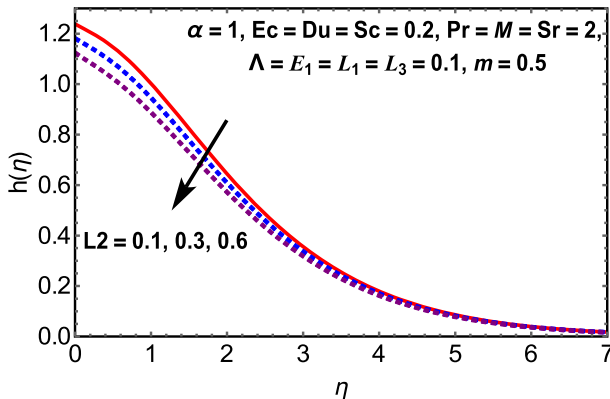

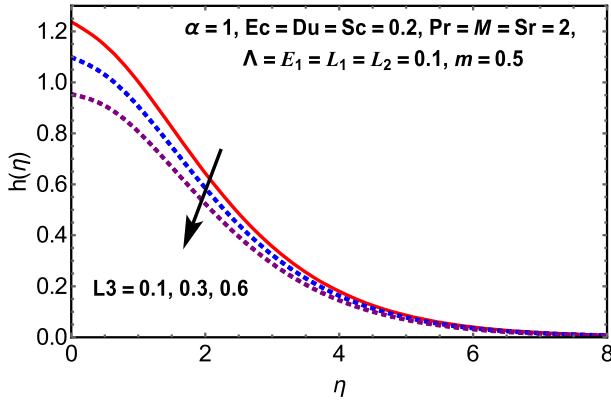**Fig. 12** Effect of thermal slip parameter L_2 on dimensionless concentration

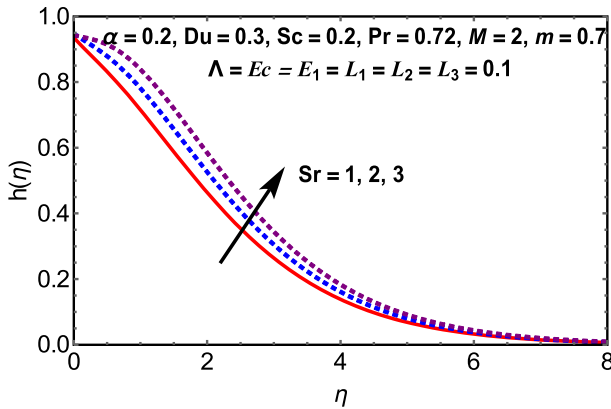**Fig. 13** Effect of diffusion slip parameter L_3 on dimensionless concentration

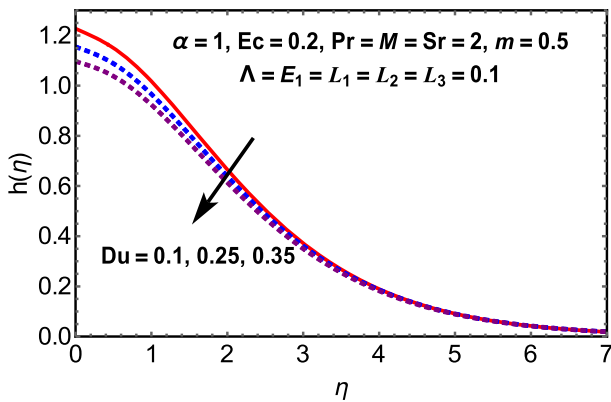**Fig. 14** Effect of Soret number Sr on dimensionless concentration

Fig. 15 Effect of Dufour number Du on dimensionless concentration

Fig. 17 demonstrates the Sherwood number which represents rate of mass transfer decreases when the Soret parameter increases as well as the concentration slip parameter L_3 increases.
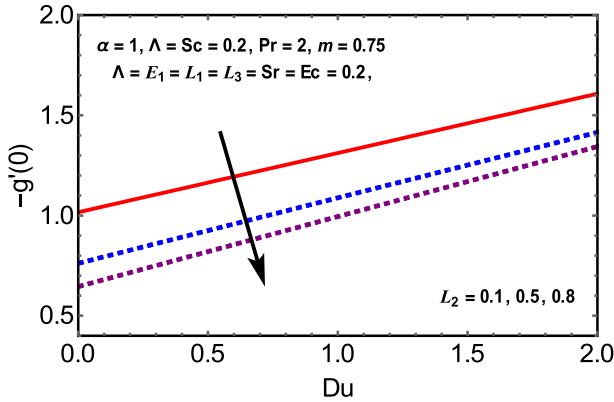
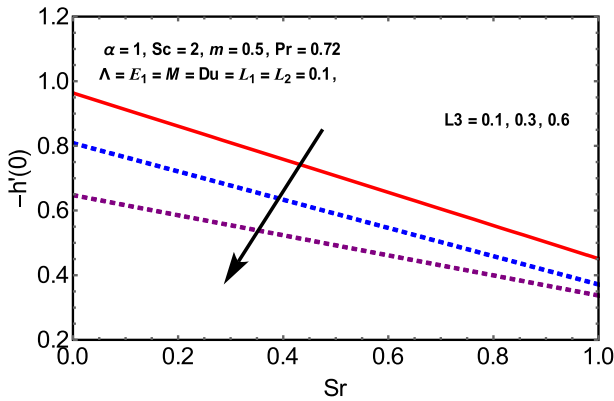**Fig. 16** Variation of Nusselt number with Du for different values of thermal slip parameter L_2

Fig. 17 Variation of Sherwood number with Sr for different values of concentration slip parameter L_3

Conclusions

In this paper, we investigated the impact of electric field, Dufour and Soret numbers on the MHD boundary layer flow of Williamson fluid over a stretching surface with variable thickness by considering slip parameters. By using similarity transformations the governing PDEs were converted into the dimensionless ordinary differential equations. We solved the transformed equations analytically using OHAM. The graphical illustrations of our results from the influence of relevant parameters on temperature, concentration and velocity profiles are argued in depth. Some of the specific conclusions which have been derived from the study can be concluded as follows:

- The semi-analytic method OHAM is effective, clear, consistent and efficient.
- Controlling and adjusting the convergence of the series solution using the convergence parameters are very simple.
- Velocity and temperature increase with an increase in the electric field.
- Increasing the magnetic field parameter M declines the velocity field initially and after some time it becomes increasing significantly.
- The heat transfer rate boosted up with an increment of Dufour number Du.

80 Page 20 of 22

Int. J. Appl. Comput. Math (2019) 5:80

- An increase in Soret number Sr reduces the mass transfer rate and intensifies the heat transfer rate.
- Velocity slip parameter L_1 rises the temperature but depreciates the velocity field.

Compliance with Ethical Standards

References

1. Tewfik, O.E., Eckert, E.R.G., Jurewicz, L.S.: Diffusion-thermo effects on heat transfer from a cylinder in cross flow. AIAA J. **1**(7), 1537–1543 (1963)
2. Ybarra, P.L.G., Velarde, M.G.: The role of Soret and Dufour effects on the stability of a binary gas layer heated from below or above. Geophys. Astrophys. Fluid Dyn. **13**, 83–94 (1979)
3. Hartranft, R.J., Sih, G.C.: The influence of the Soret and Dufour effects on the diffusion of heat and moisture in solids. Int. J. Eng. Sci. **18**, 1375–1383 (1980)
4. Garcia-Ybarra, P., Nicoli, C., Clavin, P.: Soret and dilution effects on premixed flames. Combust. Sci. Technol. **42**, 87–109 (1984)
5. Vogelsang, R., Hoheisel, C.: The Dufour and Soret coefficients of isotopic mixtures from equilibrium molecular dynamics calculations. J. Chem. Phys. **89**, 1588–1591 (1988)
6. Mohan, H.: The Soret effect on the rotatory thermosolutal convection of the veronis type. Indian J. Pure Appl. Math. **27**(6), 609–619 (1996)
7. Postelnicu, A.: Influence of a magnetic field on heat and mass transfer by natural convection from vertical surfaces in porous media considering Soret and Dufour effects. Int. J. Heat Mass Transf. **47**, 1467–1472 (2004)
8. Postelnicu, A.: Influence of chemical reaction on heat and mass transfer by natural convection from vertical surfaces in porous media considering Soret and Dufour effects. Heat Mass Transf. **43**, 595–602 (2007)
9. Alam, M.S., Rahman, M.M.: Dufour and Soret effects on MHD free convective heat and mass transfer flow past a vertical porous flat plate embedded in a porous medium. J. Nav. Arch. Mar. Eng. **1**, 55–65 (2005)
10. Cheng, C.-Y.: Soret and Dufour effects on natural convection heat and mass transfer from a vertical cone in a porous medium. Int. Commun. Heat Mass Transf. **36**, 1020–1024 (2009)
11. Cheng, C.-Y.: Soret and Dufour effects on natural convection boundary layer flow over a vertical cone in a porous medium with constant wall heat and mass fluxes. Int. Commun. Heat Mass Transf. **38**, 44–48 (2011)
12. Raju, C.S.K., Babu, M.J., Sandeep, N., Sugunamma, V., Reddy, J.V.R.: Radiation and Soret effects of MHD nanofluid flow over a moving vertical moving plate in porous medium. Chem. Process. Eng. Res. **30**, 9–23 (2015)
13. Reddy, M.G., Sandeep, N.: Free convective heat and mass transfer of magnetic bio-convective flow caused by a rotating cone and plate in the presence of nonlinear thermal radiation and cross diffusion. J. Comput. Appl. Res. Mech. Eng. **7**(1), 1–21 (2017)
14. Reddy, N., Gnaneswara Sandeep, M., Saleem, S., Mustafa, M.T.: Magnetohydrodynamic bio-convection flow of Oldroyd-B nanofluid past a melting sheet with cross diffusion. J. Comput. Theor. Nanosci. **15**(4), 1348–1359 (2018)
15. Reddy, M.G.: Cattaneo–Christov heat flux effect on hydromagnetic radiative Oldroyd-B liquid flow across a cone/wedge in the presence of cross-diffusion. Eur. Phys. J. Plus **133**, 24 (2018)
16. Williamson, R.V.: The flow of pseudo plastic materials. Ind. Eng. Chem. **21**, 1108–1111 (1929)
17. Khan, W., Khan, I., Gul, T., Idrees, M., Islam, S., Denni, L.C.C.: Thin film Williamson nanofluid flow with varying viscosity and thermal conductivity on a time-dependent stretching sheet. Appl. Sci. **6**, 334 (2016)
18. Kho, Y.B., Hussanan, A., Mohamed, M.K.A., Sarif, N.M., Ismail, Z., Salleh, M.Z.: Thermal radiation effect on MHD Flow and heat transfer analysis of Williamson nanofluid past over a stretching sheet with constant wall temperature. J. Phys. Conf. Ser. **890**, 1–6 (2017)

19. Krishnamurthy, M.R., Prasannakumara, B.C., Gireesha, B.J., Gorla, R.S.R.: Effect of chemical reaction on MHD boundary layer flow and melting heat transfer of Williamson nanofluid in porous medium. Eng. Sci. Technol. Int. J. **19**, 53–61 (2016)

20. Mabood, F., Ibrahim, S.M., Lorenzini, G., Lorenzini, E.: Radiation effects on Williamson nanofluid flow over a heated surface with magnetohyderodynamics. Int. J. Heat Technol. **35**(1), 196–204 (2017)

21. Gorla, R.S., Gireesha, B.J.: Dual solutions for stagnation-point flow and convective heat transfer of a Williamson nanofluid past a stretching/shrinking sheet. Heat Mass Transf. **52**, 1153–1162 (2016)

22. Lee, L.L.: Boundary layer over a thin needle. Phys. Fluids **10**(4), 822–868 (1967)

23. Devi, S.P.A., Prakash, M.: Temperature dependent viscosity and thermal conductivity effects on hydro-magnetic flow over a slendering stretching sheet. J. Niger. Math. Soc. **34**(3), 318–330 (2015)

24. Devi, S.P.A., Prakash, M.: Thermal radiation effects on hydromagnetic flow over a slendering stretching sheet. J. Braz. Soc. Mech. Sci. Eng. **38**, 423–431 (2015). https://doi.org/10.1007/s40430-015-0315-7

25. Babu, M.J., Sandeep, N.: MHD non-Newtonian fluid flow over a slendering stretching sheet in the presence of cross-diffusion effects. Alex. Eng. J. **55**(3), 2193–2201 (2016)

26. Reddy, S., Kishan, N., Rashidi, M.M.: MHD flow and heat transfer characteristics of Williamson nanofluid over a stretching sheet with variable thickness and variable thermal conductivity. Trans. A. Razmadze Math. Inst. **171**, 195–211 (2017)

27. Kothandapani, M., Prakash, J.: The peristaltic transport of Carreau nanofluids under effect of a magnetic field in a tapered asymmetric channel: application of the cancer therapy. J. Mech. Med. Biol. **15**(3), 1–32 (2015)

28. Hayat, T., Batool, N., Yasmin, H., Alsaedi, A., Ayub, M.: Peristaltic flow of Williamson fluid in a convected walls channel with Soret and Dufour effects. Int. J. Biomath. **9**(1), 1–19 (2016)

29. Hina, S., Mustafa, M., Haya, T.: Peristaltic motion of Johnson–Segalman fluid in a curved channel with slip conditions. PLoS ONE **9**(12), 1–25 (2014)

30. Iftikhar, N., Rehman, A., Najam, M.: Features of convective heat transfer on MHD peristaltic movement of Williamson fluid with the presence of Joule heating. In: IOP Conference Series Materials Science and Engineering (2018)

31. Arshad, S., Siddiqui, A.M., Sohail, A., Maqbool, K., ZhiWu, L.: Comparison of optimal homotopy analysis method and fractional homotopy analysis transform method for the dynamical analysis of fractional order optical solitons. Adv. Mech. Eng. **9**(3), 1–12 (2017)

32. Liu, G.L.: New research direction in singular perturbation theory: artificial parameter approach and inverse perturbation technique. In: Conference of 7th Modular Mathematics and Mechanics (1997)

33. Hayat, T., Shafiq, A., Alsaedi, A.: MHD axisymmetric flow of third grade fluid by a stretching cylinder. Alex. Eng. J. **54**, 205–212 (2015)

34. Marinca, V., Herisanu, N., Bota, C., Marica, B.: An optimal homotopy asymptotic method applied to the steady flow of fourth-grade fluid past a porous plate. Appl. Math. Lett. **22**, 245–251 (2009)

35. Marinca, V., Herisanu, N.: On the flow of a Walters-type B' viscoelastic fluid in a vertical channel with porous wall. Int. J. Heat Mass Transf. **79**, 146–165 (2014)

36. Marinca, V., Herisanu, N.: An optimal homotopy asymptotic approach applied to nonlinear MHD Jeffery-Hamel flow. Math. Probl. Eng. **2011**, 1–16 (2011). https://doi.org/10.1155/2011/169056

37. Marinca, V., Herisanu, N.: The optimal homotopy asymptotic method for solving Blasius equation. Appl. Math. Comput. **231**, 134–139 (2014)

38. Mabood, F., Khan, W.A., Md. Ismail, A.I.: Optimal homotopy asymptotic method for flow and heat transfer of a viscoelastic fluid in an axisymmetric channel with a porous wall. PLoS ONE **8**, 1–8 (2013)

39. Mustafa, M.: Viscoelastic flow and heat transfer over a nonlinearly stretching sheet: OHAM solution. J. Appl. fluid Mech. **9**, 1321–1328 (2016)

40. Abdel-Wahed, M.S., Elbashbeshy, E.M.A., Emam, T.G.: Flow and heat transfer over a moving surface with non-linear velocity and variable thickness in a nanofluids in the presence of Brownian motion. Appl. Math. Comput. **254**, 49–62 (2015)

41. Adem, G.A., Kishan, N.: Slip effects in a flow and heat transfer of a nanofluid over a nonlinearly stretching sheet using optimal homotopy asymptotic method. Int. J. Eng. Manuf. Sci. **8**(1), 25–46 (2018)

42. Aliy, G., Kishan, N.: Electrical MHD viscoelastic nanofluid flow and heat transfer over a stretching sheet with convective boundary condition. Optimal homotopy asymptotic method analysis. J. Nanofluids **8**, 1–10 (2019)

43. Aliy, G., Kishan, N.: Effect of electric field on MHD flow and heat transfer characteristics of Williamson nanofluid over a heated surface with variable thickness. OHAM Solution. J. Adv. Math. Comput. Sci. **30**(1), 1–23 (2019)

44. Scarpi, I., Dapra, G.: Perturbation solution for pulsatile flow of a non-Newtonian Williamson fluid in a rock fracture. Int. J. Rock Mech. Min. Sci. **44**, 271–278 (2007)

80 Page 22 of 22

Int. J. Appl. Comput. Math (2019) 5:80

45. Beard, D.W., Walters, K.: Elastico-viscous boundary-layer flows. Proc. Camb. Philos. Soc. **60**, 667–674 (1964)
46. Sawicki, J., Maciej, G.: Effect of external electrical field on the magnetohydrodynamic fluid flow of viscous in a slot between fixed surfaces of revolution. In: AIP Conference Proceedings 1822, pp. 020013-1–10 (2017)
47. Dulikravich, G.S., Colaco, M.J.: Convective heat transfer control using magnetic and electric fields. In: International *Thermal* Science Seminar—ITSS II, ASME-ICHMT-ZSIS, pp. 133–144 (2004)
48. Marinca, V., Herisanu, N.: The optimal Homotopy Asymptotic Method. Engineering application. Springer, Switzerland (2015)
49. Khader, M.M., Meghad, A.M.: Numerical solution for boundary layer flow due to a nonlinearly stretching sheet with variable thickness and slip velocity. Eur. Phys. J. Plus **128**, 100 (2013)
50. Fang, T., Zhang, J., Zhong, Y.: Boundary layer flow over a stretching sheet with variable thickness. Appl. Math. Comput. **218**, 7241–7252 (2012)